Bulletin of the Marine Geology, Vol. 34, No. 2, December 2019, pp. 89 to 108

# Genesis and Morphotectonic Characterisation of Crescent-Shaped feature from Alcock Rise, Andaman Sea

**Sachin Kumar Tripathi[1*], Resmi Sathikumar[1], Jishnu Balagangadharan Kaustubhakumari[2], Priyanka Dey Guha[1], Soibam Ishwarchandra Meitei[1]**

[1] Marine and Coastal Survey Division, Geological Survey of India, Kolkata

[2] Marine and Coastal Survey Division, Geological Survey of India, Mangalore

Corresponding author: *stripathi208@gmail.com

(Received 08 July 2019; in revised form 18 July 2019 accepted 14 November 2019)

**ABSTRACT :** Study of 98 crescent shape depressions over Alcock Rise, Andaman Sea were reported for the first time in between water depth -500 and -2000 m using multibeam swath bathymetry data. These gigantic depressions have crescent length (CL) varies from 600 to 3800 m and width (CW) varies from 200 to 2500 m with an average central depression of 500 m. Detailed parametric characterization reveals that slope and axial ratio of these crescentic structures have no direct relationship with general shape and steepness of their escarpment. Moreover, spatial distribution of these structures show a clustering of elongated crescent with higher crescent length to width ratio in NW margin of Alcock Rise compare to centre. This change in shape from open elliptical to semicircular depression probably suggests that earlier formed open crescents were modified at later stage to semicircular depressions. As observed in the seismic data, the formation of the crescentic depressions were initiated by the normal fault in-association with major dextral transform fault and subsequently its geometry was modified by local transpression along with seismicity induced slumping and bottom current scouring from the weaker zones. So, tectonics and bottom current activity provides simpler explanation for the formation of crescentic structure over Alcock Rise.

**Keywords:** Crescentic depression, Alcock Rise, Swath bathymetry, Bottom current, Normal fault.

## INTRODUCTION

Crescent shaped depressions have been identified in the sea-bottom world over by many workers (e.g. Rabinowitz and Ryan, 1970; Pickering *et al.*, 1989; Rebesco, 2005; Viana and Rebesco, 2007; Viana, 2008; Hernandez-Molina *et al.*, 2010; Casalbore *et al.*, 2015; Jacob *et al.*, 2014; Llave *et al.*, 2015; De Leeuw *et al.*, 2016) and their mechanism of formation has always being a topic of interest for the geoscientific community. Many researchers believe that they are formed associated with contourite currents (Faugères *et al.*, 1993; Rebesco and Stow, 2001; Laberg *et al.*, 2001; Stow *et al.*, 2002; Rebesco, 2005; Hernández-Molina *et al.*, 2006; Mulder *et al.*, 2006; Hanquiez *et al.*, 2007; García *et al.*, 2009; Van Rooij *et al.*, 2010; Casalbore *et al.*, 2014; Rebesco *et al.*, 2014; Hernández-Molina *et al.*, 2014a) and some consider their formation by the pockmarks associated with fluid escape processes (King and MacLean, 1970; Hovland, 1989; Somoza *et al.*, 2003; Rensbergen *et al.*, 2005; Judd and Hovland, 2007; Collins *et al.*, 2011). However, many believe that these submarine crescent shaped morphologies are related to erosional process such as scouring bottom current activity and mass wasting (Bonnel *et al.*, 2005; Rebesco and Camerlenghi, 2008; Maldonado *et al.*, 2003; Stow *et al.*, 2009; Van Rooij *et al.*, 2010; Rebesco *et al.*, 2014; Hillman *et al.*, 2018). Few other geoscientists noticed that crescent shape features were formed by the termination of the submarine channels (Bulat and Long, 2001; Verdicchio and Trincardi, 2006; Fildani *et al.*, 2006). Moreover, detailed information regarding formation of crescentic depression was discussed by Duarte *et al.* (2010) from deeper water depth (-4300 m) and García *et al.* (2015) from middle slope between -500 to -1200 m water depth of the north eastern part of the Gulf of Cadiz. Similar crescentic geomorphic depressions were recorded for the first time from Andaman Sea in recently acquired swath bathymetry, sub-bottom profiler and on earlier available multi-channel seismic section (Katari *et al.*, 2015) over tectonically active Alcock Rise. The present work aims to understand the genesis of these geomorphic features by detailed morphological analysis and determination of their internal sedimentary structure, and also to discuss the different processes that could have led to their formation over Alcock Rise.

## GEOLOGICAL FRAMEWORK

Andaman Sea is a complex back-arc extensional basin formed by transtension and lying along a highly oblique convergent margin of overriding Southeast Asian plate and the subducting Australian plate (McCaffery, 1992; Curray, 2005; Kamesh Raju, 2005 and Cochran, 2010). Oblique convergence has been

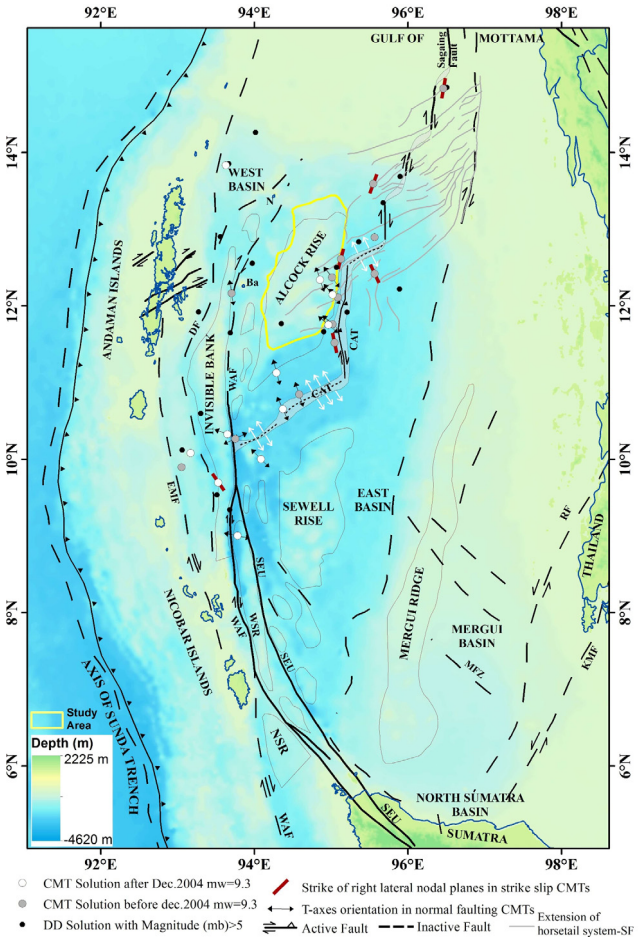


Figure 1. Map depicts tectonics disposition of major lineaments in the Andaman Sea. Abbreviations for this figure: Ba= Barren Island, N = Narcondam Island, DF = Diligent Fault, EMF= Eastern Margin Fault, NSR = North Sumatra Ridge, , SEU = Seulimeum fault, WAF= West Andaman Fault, CAT= Central Andaman Trough, White arrow shows extension regime within the CAT spreading axis (After Curray, 2005 and Diehl *et al.* 2013).

responsible for the formation of a sliver plate between the subduction zone and a complex right-lateral fault system (Curray, 2005). Late Paleocene convergence started clockwise rotation and bending of the northern and western Sunda Arc. The initial sliver fault probably started in the Eocene and extended through the outer arc ridge offshore from Sumatra through the present region of the Andaman Sea into the Sagaing Fault (Curray, 2005; Kamesh Raju 2005). Due to increased strike-slip motion, series of extensional basins opened in form of back-arc extension. This extensional opening resulted different geomorphic domain from west to east and also dissected by different scale of tectonic lineaments. The outer arc ridge is separated from fore-arc basin (mainly West Basin, Invisible Bank and West Sewell Ridge) by Diligent Fault (DF) and Eastern Margin fault (EMF) system. However, Back-arc region mainly Inner arc volcanic, Alcock Rise, Sewell Rise, East Basin and Central Andaman Trough (CAT) is separated from the fore-arc basin by West Andaman Fault (WAF) and Sumatran fault system (SFS). It is also reported that the N-S trending WAF is dominantly strike-slip in the central and southern sector (Curray, 2005). Further south, a mixed response of strike-slip as well as thrust-fault motions is recorded and giving rise to an array of seismicity particularly at the junction of WAF and spreading zones south of 8° N (Kamesh Raju *et al.*, 2004; and Curray, 2005). The WAF is running more or less N-S direction as a major tectonic feature other than Sagaing fault and ultimately merges with SFS near Great Nicobar and finally abutting against the Sunda Subduction Zone (Curray *et al.*, 1979; and Taira, 1983; Figure 1). Sagaing fault merges with the WAF in the west part of the CAT near 8° N and controls seismicity around Alcock Rise (Diehl *et al.*, 2013). Alcock Rise is a part of a backarc basin and came into existence around 23-15 Ma (Kamesh Raju, 2005; Curray, 2005). Geology of Alcock and Sewell Rise is very complex; various researchers have different opinion regarding its origin and tectonics. Rodolfo (1969), Kamesh Raju (2005) and Curray (2005) pointed out that part of Alcock Rise is comprised of typical backarc basin tholeiitic basalt, formed as a result of sea floor spreading in the Alcock and Sewell regions. Morley and Alvey (2015), however opined that the volcanic samples from the Alcock Rise were extruded onto hyper-extended continental crust and do not represent the part of the oceanic crust formation. Moreover, limestone rock fragment of early Miocene age from the southeastern part of Alcock Rise (Tripathi and Banerjee, 2016) suggests that this might have formed above the early-crystallized basement rock. These rock pieces may be directly linked with the formation of Alcock and Sewell rise during entire journey of Andaman opening. Initially, extension episode of the Andaman Sea was WNW-ESE during late Palaeogene with highly oblique extension (NNW-SSE) during Neogene (Morley, 2017) and north-south ridge system that opened the eastern Andaman Sea by drifting from the main land of Malay Peninsula during early Tertiary (Curray, 2005). In early Oligocene, the plate edge thought to be the Sagaing Fault (SF) was directly connected with the old WAF (Curray, 2005). Moreover, Mergui Basin and North Sumatra Basin (Figure 1) were also formed during this period. During 23-15 Ma period, backarc area of Andaman Sea witnessed formation of conjoined Alcock and Sewell Rise and at same time, top of the Andaman-Nicobar Island also emerged above the sea level (Curray, 2005). Subsequently during 15-4 Ma period, the Eastern Margin and Diligent Faults may have been active and WAF was probably inactive in west of Alcock and

Sewell Rise (Curray, 2005; Figure 1). Later conjoined Alcock and Sewell Rises started rifting away from each other and resulted deep basin complex CAT at about 4 Ma, which still continuous in the NE-SW direction (Kamesh Raju, 2005 and Curray, 2005).

## NEOTECTONICS AND SEISMICITY OF ALCOCK RISE

Neotectonics and seismic activity of the central region of the Andaman Sea recorded maximum earthquake (5.0Mb and 9.3Mb) which is mainly concentrated along N-S SF and rift elements in both northern and southern part of the Alcock Rise, (Diehl *et al.*, 2013; Figure 1). Moreover, Alcock Rise is locked within the active right-lateral strike-slip and NE-SW normal faults that connect the right-lateral Sumatra, Seulimeum and WAF in the southwest and with SF in the northeast (Figure 1, Curray, 2005; Cochran, 2010). Adjacent to Alcock Rise, two segments of spreading centers located at 10˚N and 14˚N are separated by right lateral N-S transform fault (Figure 1, Eguchi *et al.*, 1979). Between these two spreading centers, earthquakes also recorded along NE-SW striking structure which is the trend of fault strike near the Alcock Rise 12.4˚N/95˚E and 12.8˚N/95.5˚E (Diehl *et al.*, 2013). According to Diehl *et al.* (2013), majority of earthquakes in backarc region are recorded along the extensional plate boundary in the CAT compared to the intraplate of the backarc region (Figure 1). Earthquakes along the fault system connecting the CAT with the SF in the northeastern backarc are scattered but bigger ( 5.0mb) relative to the CAT ( 5.0mb, Diehl *et al.*, 2013). Earthquake clusters at 12.4˚N/95˚E and 11.8˚N/95.5˚E in east of the Alcock Rise are associated with 1983 and 1984, 2003 earthquakes and these clusters were recorded from NE-SW striking extensional fault zone (Rangin *et al.*, 1999; Diehl *et al.*, 2013). These earthquake swarms in 1983 and 1984 events at 12.8˚N/95.5˚E is indicative of active spreading processes involved in the formation of extension basin in the further north of Alcock Rise near 14˚N (Seeber *et al.*, 2006, Diehl *et al.*, 2013).

## OCEANOGRAPHIC SETTING OF NORTH ANDAMAN SEA

Andaman Sea can be considered as a separate sea to some extent and it is connecting to the equatorial ocean and Bay of Bengal (BoB) by three primary passages (Figure 2) mainly southern great Nicobar channel (SC: 6˚N, 1200-1500 m deep) between the southernmost part of the Nicobar Islands and the northern tip of Sumatra. Second, middle channel known as ten-degree channel (MC: 10˚N, 600-800 m deep) is separating the Andaman Islands and Nicobar Islands and third northern Preparis channel (15˚N, 400-500 m deep) separates the Andaman ridges with Myanmar Island. Andaman Sea also receives current through Java Sea, southern part of South China Sea. A small part of equatorial current enters Andaman Sea mainly through SC and MC during spring and propagates eastward along western boundary of Thailand and exit to the bay through NC. However, smaller part of equatorial internal current is also flowing southward along the east coast of the Andaman Islands and exit to the bay via the MC (Osborne and Burch, 1980; Cheng *et al.,* 2013; Potemra *et al.*, 1991; Hsu *et al.*, 2014). Apart from this, several pockets of strong internal soliton current mechanism in Andaman Sea are also producing through fission process due to the extremely varied topography like Alcock, Sewell Rise and along the east of the Andaman

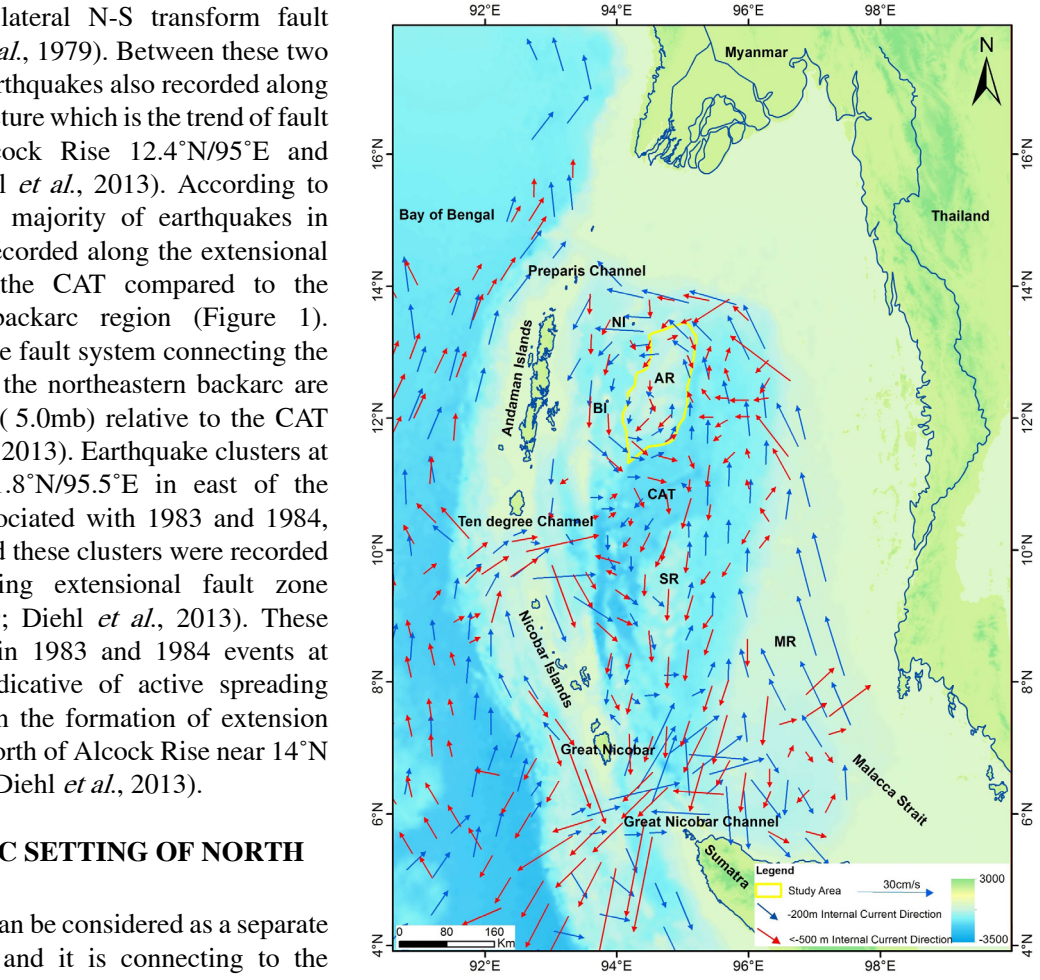


Figure. 2 Map depicts internal current flow pattern in the Andaman Sea. Abbreviations for this figure: BI= Barren Island, NI = Narcondam Island, AR= Alcock Rise, SR = Sewell Rise, MR = Mergui Ridge, CAT= Central Andaman Trough, (Modified after Chatterjee *et al., 2017;* and Sun *et al.,* 2019).

and Nicobar Islands (Hyder *et al.*, 2005; Mohanty and Devendra, 2017). According to Chatterjee *et al.* (2017), circulation of current in the Andaman Sea is fairly complex and distinct eddy form to the north and south of the MC at the surface as well as subsurface levels (Figure 2) where large tidal current oscillate across shallow steep bathymetry through nonlinear processes. Internal waves in the Andaman Sea may occur every day; however, they occur more often after a new moon and full moon (Chatterjee *et al.*, 2017). Similar multiple internal wave trains are also noticed by the Sun *et al.* (2019) and they observed several strong internal wave pockets are propagating in different directions and the direction variability is mainly controlled by bottom topography features and their wave fronts are parallel to local isobaths (Osborne and Burch, 1980). The large amount of internal wave activity is noticed year-round in the northern Andaman Sea and these internal waves spread outward with irregular arc radiations from the source and disintegrate in the process of their transmission. Accordingly, two columns of groups of internal waves are propagating in northern part of the Andaman Sea (Figure 2). One southeast propagating wave originates near the northern Andaman Sea and the southwestern propagating waves originate at the continental slope of the northern Andaman Sea (Sun *et al.*, 2019).

## MATERIAL AND METHODS

Identification and description of crescentic depressions resulted from the analysis of four main sets of data: multibeam echosounder swath bathymetry (MBES), sub-bottom profiler (SBP), 2D multichannel seismic reflection and Acoustic Doppler Current Profiler (ADCP) data. The swath bathymetry data were used to characterize the geomorphology of the area where the crescentic depressions are situated and also to accomplish a detailed morphological characterization of these features. Along with swath bathymetry, SBP dataset reflects the subsurface morphology of up to 40 m sediments below the seafloor over these depressions and also used for analyzing fluid migration study. Along with these data, earlier acquired multichannel seismic reflection dataset (Katari *et al.*, 2015) was also used. Data was processed by Promax 2D Software vision 8.2.1. with vertical resolution of 5m to 10m and further the process data was used to unravel the deep seated structure present below the crescentic depressions. The recorded set of data was obtained using two set of airguns as the seismic source and provided higher penetrations (up to 2.0s TWT).

Multibeam swath bathymetry dataset was acquired during field season programme of Geological Survey of India, onboard R.V. Samudra Ratnakar in 2017, and covered part of the Alcock Rise, Central Andaman Trough and part of West Basin (Figure 1). Reson Sea Bat 7150-7-P Multichannel Echosounder Reson Pvt. Ltd, of Denmark makes has been used for real time data acquisition during swath bathymetric survey. It operates with 12 kHz transducer frequency. The acquired MBES data has been processed to eliminate all the noises with various filter options that are available in PDS 2000 software and final grid model was prepared on 30m pixel size. Later processed grid model was analysed in Arc-GIS platform for better terrain analysis and interpretation.

To generate more information regarding erosion, deposition and fluid migration nature within the crescent shaped depressions, SES-2000 deep system manufactured by Innomar Technologie GmbH, Rostock, Germany, was used at 4 kHz secondary frequency to achieve extended range and penetration with better resolution in centimetre through SESWIN (Sediment Echo Sounder for Windows) software. During the survey, multi-ping mode and lower frequency channel has been used to reduce the signal to noise ratio. Similarly, stacking and smoothing options were also applied to improve the signal to noise ratio along with median filter. Thereafter, acquired raw data was processed through interactive sediment editor (ISE) post processing software. Along with these instruments, hull mounted Teledyne RD instrument make Ocean Observer ADCP was also deployed and data acquired through the VMDAS (RD instrument) interface software with a set frequency of 150kHz following the working principle of the doppler effect of sound waves for study of the current pattern and their dimensions over the Alcock Rise. Acquired data was processed using the win ADCP software. To know the effect of bottom current over sediment in depression area, samples were collected through spade core and classified visually based on the grain size. With the help of above data set, the formation of crescentic depressions over Alcock Rise were studied in detail utilizing different morphological parameters as described by Duarte *et al.* (2010) such as escarpment width (EW), escarpment height (EH), slope, dip of the escarpment (angle between EH and EW), crescent length (CL) and crescent width (CW).

## RESULTS

Detailed swath bathymetric map (Figure 3) and current analysis map (see supplementary data Figure S1 and Figure S2) were prepared, which reveals different controlling factors assisting in the development of numerous crescentic depressions over gentle slope of the Alcock Rise. Each component that are contributing the formation of these crescent features are discussed below.

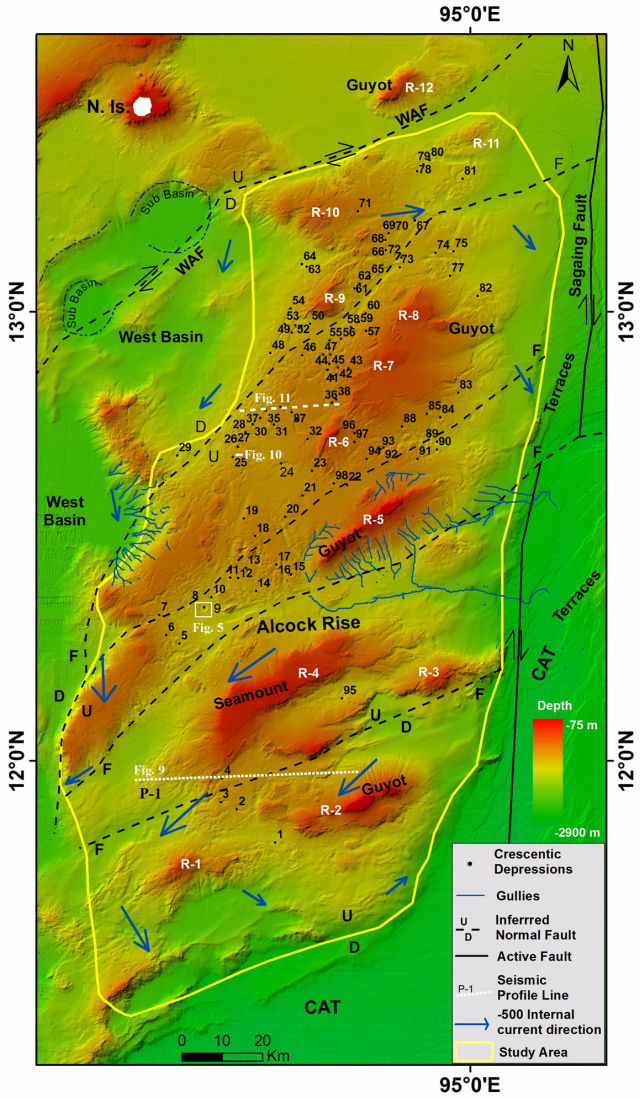


Figure 3. Crescent shaped depressions over Alcock Rise, Andaman Sea (CAT- Central Andaman Trough, N.Is. - Narcondam Island, P-1 seismic profile).

## Geomorphology of the Alcock Rise

Swath bathymetric analysis reveals distinct geomorphic elements within and around study area such as seamounts, guyots, different order of drainage (channels), elliptical to semi-circular depression, unpaired terraces within the deep basin of CAT with many major linear structures (e.g. SF, NE-SW normal fault Figure 1 and Figure 3). A structural high is witnessed in swath bathymetry map such as Narcondam volcanic Island, guyots in the north part and NE-SW to NNE -SSW trending different seamounts and Guyots over Alcock Rise (R-1 to R-12, Figure 3). It is also observed that the geometry of seamounts and guyots system (R-1 to R-12) changes from south to north. In southern part the trend of the seamount and guyots (R-1 to R-5) are NE-SW and it (R-6 to R-12) becomes NNE-SSW in northern part of the Alcock Rise (Figure 3). The slopes of these guyots are steep up to 75˚ (Figure 4). Within these topographic highs, there are intermittent valley areas following the trend of the rises. Apart from these geomorphic highs, several sub-basins were also observed within the West Basin (Figure 3). Another geomorphic feature observed further east and south of the study area is having unpaired terraces with sharp change in slope between 10˚ to 25˚ (Figure 3 and Figure 4). Numerous symmetrical gullies are also recognized with varying dimension, which comes down from high seamounts and guyots (Figure 3) and their combined outlets are debouching into the CAT, while the different order of streams on western parts are also debouching over gentle slope of the Alcock Rise and finally merges into the West Basin (Figure 3). Apart from this, the gentle slope of Alcock Rise comprises numerous elliptical to crescentic shaped depressions of varying dimensions and shape within the water depth of -800 to -2000m (Figure 3).Two profiles were taken over two different morphometric crescent depressions number 9 and 33. Crescent depression 9 exhibits depression along the margin with central raised portion with an average depth of 80m and diameter more than 1000m, gradient of this crescent is ~2˚ in SW direction and ~3˚ in NE

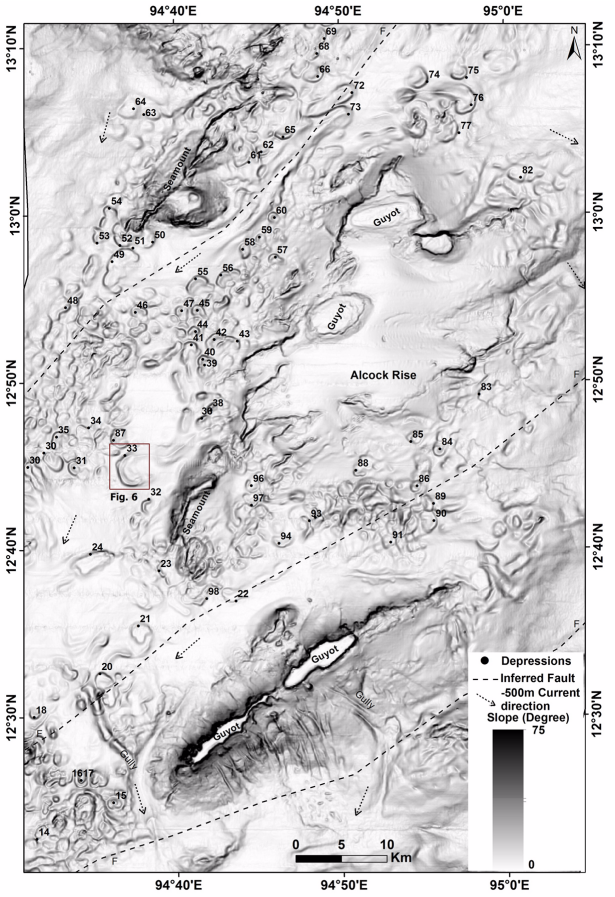


Figure 4. Slope map of the study area with location of different crescentic depressions.

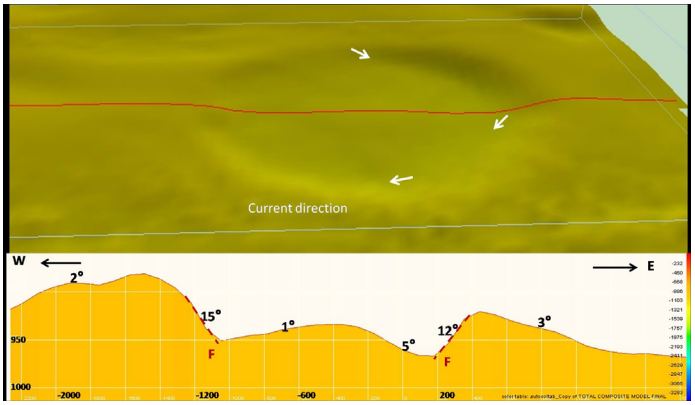


Figure 5. Morphometric parameters of crescentic depression (No. 9) from central part of the area.

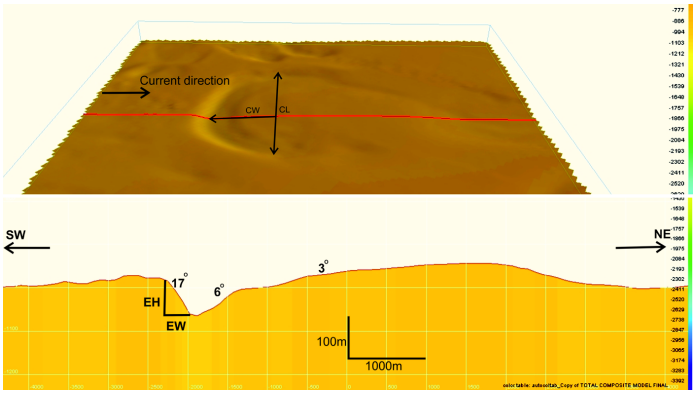


Figure 6. Morphometric parameters of crescentic depression (No. 33) from northern part of the area.

direction with steep gradient around 15˚ and 12˚ (Figure 5). Although, profile is crossing over depression number 33 shows a gentle gradient (~3˚) on southwestern side and steeper (~17˚) on northeastern side (Figure 6). It also noticed that, majority of the crescent depression on northwestern slope of Alcock Rise exhibit opening of the crescent depression is towards west. Few crescentic depressions (9, 47 and 71) at places lose their crescentic nature and form almost circular shape (Depression number 9, Figure 3). As mentioned in the method section, these 98 crescentic depression features were analyzed using different morphometric parameters over the Alcock Rise.

## Morphometry of the crescentic depressions

The results of the morphometric analysis of crescentic depressions are summarized in Table 1. This analysis revealed that escarpments present values of EH and EW varying between 20 to 110 m and 100 to 1500 m, respectively. Measured mean slope of these features is around 0.20$^{o}$ with standard deviation of 0.006$^{o}$ and the average dip around 11$^{o}$ (Table-1). However, maximum slope shown by the depressions is 0.39$^{o}$ with a maximum dip of around 22$^{o}$ . The crescentic axial depressions are characterized by CW that varies from 200 to 2500m and CL is varying between 600 and 3800m (Figure 7 and Table-1). Based on the formula used by Duarte *et al.* (2010), axial ratio 'a' was calculated by dividing half of the length (CL) with width (CW) and plotted against each other (Figure 7). Where, 5% data represent axial ratio value 'a' is equal 1 and this category belongs to approximates semicircular depressions. Moreover, 47% of depressions present semi-elliptical shapes with CL/2>CW, i.e., more elongated along CL. This group of crescentic features is mainly located in NW sector of the study area. Whereas remaining 48% of the depressions falls in the semi-elliptical shape with CL/2<CW showing elongation towards CW and this data is scattered overall. Further, relation between slope and axial ratio of crescentic depressions clustered in three groups as a function

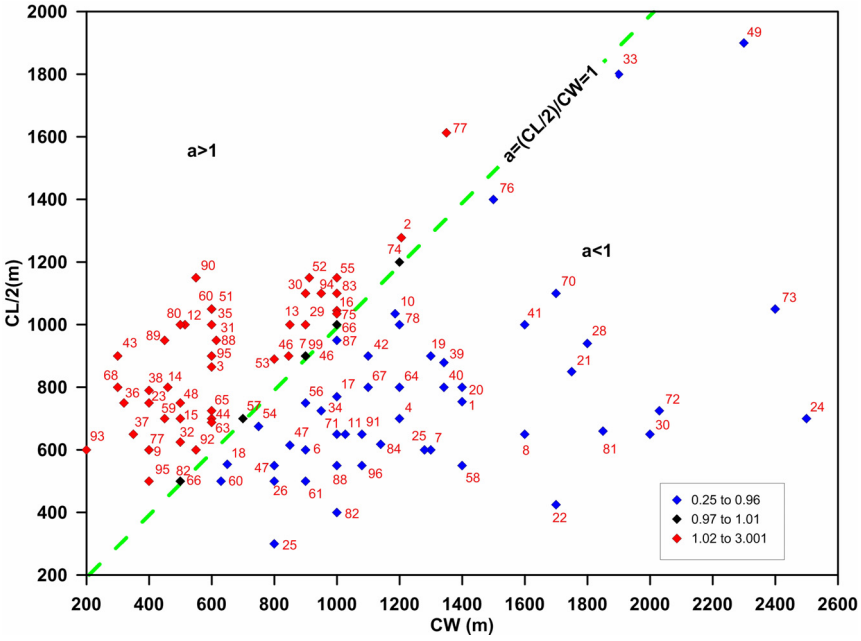


Figure 7. Morphological parameterization of the studied crescentic depressions. Graphic display of CL/2 versus CW (parameter a) for the studied features (dashed line corresponds to CL/2=CW).

Table-1. Different parameters of crescentic depression over Alcock Rise Andaman Sea (CL: Crescent Length; CW: Crescent Width, EW: Escarpment Width, EH: Escarpment Height, Axial Ratio (a): (CL/2)/CW), D:Dip in angle]

| Sl no | CL (m) | CW (m) | EW (m) | EH (m) | D | CL/2 | a | Slope (°) | Sl no | CL (m) | CW (m) | EW (m) | EH (m) | D | CL/2 | a | Slope (°) |
|---|---|---|---|---|---|---|---|---|---|---|---|---|---|---|---|---|---|
| 1 | 1508 | 1400 | 400 | 50 | 7 | 754 | 0.54 | 0.126 | 51 | 2100 | 600 | 200 | 70 | 9 | 1050 | 1.75 | 0.162 |
| 2 | 2555 | 1206 | 500 | 80 | 10 | 1277 | 1.06 | 0.18 | 52 | 2300 | 912 | 400 | 60 | 16 | 1150 | 1.26 | 0.288 |
| 3 | 1730 | 600 | 200 | 80 | 21 | 865 | 1.44 | 0.378 | 53 | 1780 | 800 | 400 | 70 | 16 | 890 | 1.11 | 0.288 |
| 4 | 1400 | 1200 | 300 | 100 | 11 | 700 | 0.58 | 0.198 | 54 | 1350 | 750 | 250 | 60 | 15 | 675 | 0.9 | 0.27 |
| 5 | 1200 | 1300 | 800 | 80 | 3 | 600 | 0.46 | 0.054 | 55 | 2300 | 1000 | 300 | 60 | 11 | 1150 | 1.15 | 0.198 |
| 6 | 1200 | 900 | 270 | 50 | 12 | 600 | 0.67 | 0.216 | 56 | 1500 | 900 | 300 | 50 | 12 | 750 | 0.83 | 0.216 |
| 7 | 1200 | 400 | 400 | 50 | 14 | 600 | 1.5 | 0.252 | 57 | 1400 | 700 | 250 | 50 | 13 | 700 | 1 | 0.234 |
| 8 | 1300 | 1600 | 500 | 80 | 10 | 650 | 0.41 | 0.18 | 58 | 1100 | 1400 | 300 | 60 | 12 | 550 | 0.39 | 0.216 |
| 9 | 1800 | 900 | 400 | 40 | 13 | 900 | 1 | 0.234 | 59 | 1400 | 450 | 200 | 50 | 11 | 700 | 1.56 | 0.198 |
| 10 | 2070 | 1186 | 600 | 60 | 4 | 1035 | 0.87 | 0.072 | 60 | 1000 | 630 | 200 | 50 | 12 | 500 | 0.79 | 0.216 |
| 11 | 1300 | 1027 | 500 | 55 | 7 | 650 | 0.63 | 0.126 | 61 | 1000 | 900 | 300 | 60 | 12 | 500 | 0.56 | 0.216 |
| 12 | 2000 | 515 | 200 | 50 | 10 | 1000 | 1.94 | 0.18 | 62 | 1000 | 500 | 250 | 60 | 13 | 500 | 1 | 0.234 |
| 13 | 2000 | 850 | 200 | 40 | 16 | 1000 | 1.18 | 0.288 | 63 | 1375 | 600 | 300 | 40 | 4 | 687 | 1.15 | 0.072 |
| 14 | 1600 | 460 | 500 | 40 | 12 | 800 | 1.74 | 0.216 | 64 | 1600 | 1200 | 300 | 70 | 13 | 800 | 0.67 | 0.234 |
| 15 | 1400 | 500 | 800 | 80 | 6 | 700 | 1.4 | 0.108 | 65 | 1450 | 600 | 200 | 70 | 17 | 725 | 1.21 | 0.306 |
| 16 | 2089 | 1000 | 200 | 60 | 18 | 1044 | 1.04 | 0.324 | 66 | 2000 | 1000 | 200 | 40 | 12 | 1000 | 1 | 0.216 |
| 17 | 1540 | 1000 | 1000 | 110 | 9 | 770 | 0.77 | 0.162 | 67 | 1600 | 1100 | 300 | 70 | 14 | 800 | 0.73 | 0.252 |
| 18 | 1107 | 650 | 400 | 60 | 13 | 553 | 0.85 | 0.234 | 68 | 1600 | 300 | 100 | 30 | 12 | 800 | 2.67 | 0.216 |
| 19 | 1800 | 1300 | 800 | 20 | 3 | 900 | 0.69 | 0.054 | 69 | 2100 | 600 | 200 | 30 | 11 | 1050 | 1.75 | 0.198 |
| 20 | 1600 | 1400 | 300 | 70 | 15 | 800 | 0.57 | 0.27 | 70 | 2200 | 1700 | 150 | 50 | 18 | 1100 | 0.65 | 0.324 |
| 21 | 1700 | 1750 | 600 | 50 | 4 | 850 | 0.49 | 0.072 | 71 | 1300 | 1000 | 200 | 20 | 9 | 650 | 0.65 | 0.162 |
| 22 | 850 | 1700 | 300 | 25 | 5 | 425 | 0.25 | 0.09 | 72 | 1450 | 2030 | 600 | 80 | 5 | 725 | 0.36 | 0.09 |
| 23 | 1500 | 400 | 200 | 40 | 10 | 750 | 1.88 | 0.18 | 73 | 2100 | 2400 | 200 | 80 | 6 | 1050 | 0.44 | 0.108 |
| 24 | 1400 | 2500 | 1000 | 70 | 13 | 700 | 0.28 | 0.234 | 74 | 2400 | 1200 | 400 | 80 | 11 | 1200 | 1 | 0.198 |
| 25 | 600 | 800 | 400 | 60 | 8 | 300 | 0.38 | 0.144 | 75 | 2070 | 1000 | 500 | 60 | 10 | 1035 | 1.04 | 0.18 |
| 26 | 1000 | 800 | 400 | 35 | 13 | 500 | 0.63 | 0.234 | 76 | 2800 | 1500 | 400 | 60 | 11 | 1400 | 0.93 | 0.198 |
| 27 | 1200 | 1280 | 400 | 60 | 15 | 600 | 0.47 | 0.27 | 77 | 3225 | 1350 | 300 | 80 | 15 | 1612. | 1.19 | 0.27 |
| 28 | 1880 | 1800 | 300 | 40 | 12 | 940 | 0.52 | 0.216 | 78 | 2000 | 1200 | 200 | 60 | 13 | 1000 | 0.83 | 0.234 |
| 29 | 2000 | 900 | 500 | 100 | 11 | 1000 | 1.11 | 0.198 | 79 | 1800 | 900 | 600 | 40 | 4 | 900 | 1 | 0.072 |
| 30 | 2200 | 900 | 700 | 100 | 12 | 1100 | 1.22 | 0.216 | 80 | 2000 | 500 | 500 | 70 | 10 | 1000 | 2 | 0.18 |
| 30 | 1300 | 2000 | 1000 | 50 | 9 | 650 | 0.33 | 0.162 | 81 | 1320 | 1850 | 500 | 60 | 13 | 660 | 0.36 | 0.234 |
| 31 | 1900 | 615 | 100 | 60 | 15 | 950 | 1.54 | 0.27 | 82 | 800 | 1000 | 700 | 80 | 11 | 400 | 0.4 | 0.198 |
| 32 | 1250 | 500 | 400 | 50 | 15 | 625 | 1.25 | 0.27 | 83 | 2200 | 1000 | 400 | 50 | 7 | 1100 | 1.1 | 0.126 |
| 33 | 3600 | 1900 | 1500 | 60 | 13 | 1800 | 0.95 | 0.234 | 84 | 1235 | 1140 | 200 | 50 | 12 | 617 | 0.54 | 0.216 |
| 34 | 1450 | 950 | 100 | 30 | 8 | 725 | 0.76 | 0.144 | 85 | 1800 | 600 | 150 | 70 | 9 | 900 | 1.5 | 0.162 |
| 35 | 2000 | 600 | 200 | 70 | 14 | 1000 | 1.67 | 0.252 | 86 | 1000 | 500 | 500 | 60 | 9 | 500 | 1 | 0.162 |
| 36 | 1500 | 320 | 200 | 80 | 17 | 750 | 2.34 | 0.306 | 87 | 1900 | 1000 | 300 | 50 | 12 | 950 | 0.95 | 0.216 |
| 37 | 1300 | 350 | 200 | 20 | 8 | 650 | 1.86 | 0.144 | 88 | 1100 | 1000 | 300 | 60 | 7 | 550 | 0.55 | 0.126 |
| 38 | 1580 | 400 | 400 | 80 | 17 | 790 | 1.98 | 0.306 | 89 | 1900 | 450 | 500 | 40 | 8 | 950 | 2.11 | 0.144 |
| 39 | 1757 | 1342 | 200 | 60 | 12 | 878 | 0.65 | 0.216 | 90 | 2300 | 550 | 500 | 60 | 11 | 1150 | 2.09 | 0.198 |
| 40 | 1600 | 1342 | 200 | 50 | 16 | 800 | 0.6 | 0.288 | 91 | 1300 | 1080 | 250 | 50 | 13 | 650 | 0.6 | 0.234 |
| 41 | 2000 | 1600 | 300 | 60 | 16 | 1000 | 0.63 | 0.288 | 92 | 1200 | 550 | 200 | 50 | 17 | 600 | 1.09 | 0.306 |
| 42 | 1800 | 1100 | 300 | 60 | 15 | 900 | 0.82 | 0.27 | 93 | 1200 | 200 | 200 | 40 | 12 | 600 | 3 | 0.216 |
| 43 | 1800 | 300 | 400 | 50 | 9 | 900 | 3 | 0.162 | 94 | 2200 | 950 | 300 | 50 | 7 | 1100 | 1.16 | 0.126 |
| 44 | 1400 | 600 | 300 | 60 | 16 | 700 | 1.17 | 0.288 | 95 | 1000 | 400 | 500 | 100 | 9 | 500 | 1.25 | 0.162 |
| 45 | 1230 | 850 | 300 | 30 | 9 | 615 | 0.72 | 0.162 | 96 | 1100 | 1080 | 200 | 50 | 13 | 550 | 0.51 | 0.234 |
| 46 | 1800 | 846 | 800 | 40 | 9 | 900 | 1.06 | 0.162 | 97 | 1200 | 400 | 200 | 40 | 22 | 600 | 1.5 | 0.396 |
| 47 | 1100 | 800 | 200 | 40 | 13 | 550 | 0.69 | 0.234 | 98 | 1800 | 600 | 500 | 60 | 9 | 900 | 1.5 | 0.162 |
| 48 | 1500 | 500 | 300 | 90 | 16 | 750 | 1.5 | 0.288 | **Minimum** | **600** | **200** | **100** | **20** | **3** | **300** | **0.25** | **0.054** |
| 49 | 3800 | 2300 | 600 | 50 | 8 | 1900 | 0.83 | 0.144 | **Maximum** | **3800** | **2500** | **1500** | **110** | **22** | **1900** | **3.00** | **0.396** |
| 50 | 2100 | 600 | 900 | 80 | 11 | 1050 | 1.75 | 0.198 | **Average** | **1660** | **970** | **387.5** | **58.1** | **11.4** | **830** | **1.06** | **0.206** |

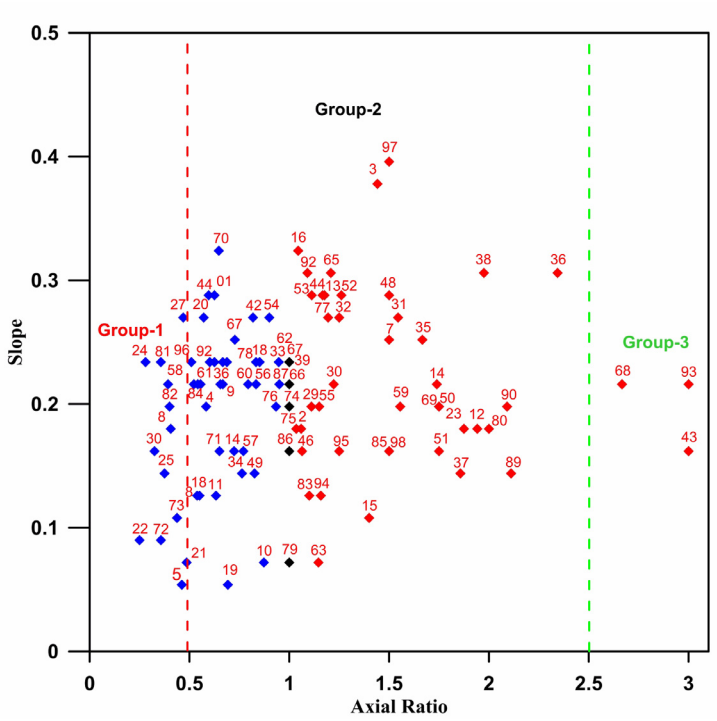


Figure 8. Bivariant diagram depicts the relationsip between slope and axial ratio of the crescentic depressions.

of their different values of 'a' (Figure 8). Group 1 consists of 13 crescentic features (mainly 5, 8, 21, 22, 24, 25, 27, 30, 58, 72, 73, 81 and 82), which exhibits a singular low 'a' value (less than 0.5), implying an extreme concavity, and a highly elongated geometry parallel to the direction of its longest CW axis (Figure 8). Group 2 includes 84% of the features, which geometry is either more elongated along CW axis or more elongated along CL axis with an axial ratio between 0.5 and 2.5. Finally, group 3 comprised of only 3 features, which exhibit highly elongated semi-elliptical shape (mainly 43, 68 and 93) with relatively high axial ratio more than 2.5 (Figure 8). Inter-relationship of EH and EW is also assessed to know the linear correlation of the formation of crescentic depressions and no such particular trend observed, as all the points are scattered.

## Sub-surface sedimentary architecture of the crescentic depressions

Structure and sedimentary architecture underneath crescentic depressions number 2, 3 and 4 is imaged in Figure 9 was taken into consideration for present study because it covers all possible morphotectonic element of the basin (Figure 9 and Figure 1). Acoustic basement underneath the Alcock Rise is characterized by high amplitude irregular and chaotic folded and faulted reflections pattern with sound velocity between 3.89 km/s to 4.60 km/s (Katari *et al.*, 2015) with a thickness of about 0.5s (TWT). It is cut by several normal faults that also affecting the overlying seismic unit A and most of them breaching out at the seafloor surface (Figure 9). Unit A is approximately 0.5s to 1s thick and underlain by discontinuity corresponding to the top basement and is trapped within graben like feature. Its internal reflections are parallel, defining a stratified pattern (Figure 9) with seismic velocity of 1.62 km/s to 3.50 km/s. Most of the reflector patterns are well stratified and have onlap terminations and are offset by the pervasive faulting. However, both basement and unit A are intersected by volcanic intrusion. Volcanic intrusion pushes entire meta-sediment in upward direction, as the reflector property over intrusive is nearly matching with basement unit (Figure 9). Another observation is noticed in form nearly acoustic transparent reflection pattern west of the intrusive and marked as mass movement (MTD) in the

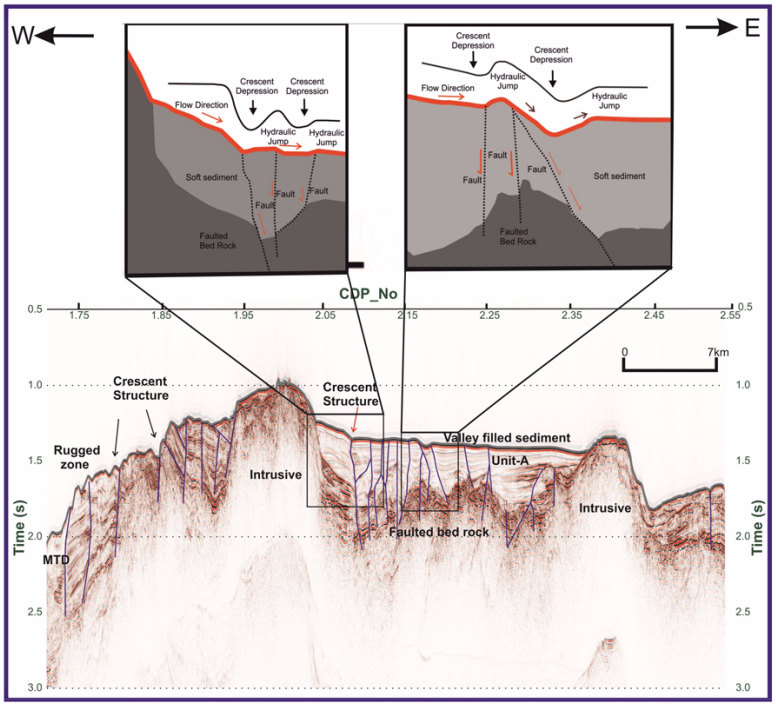


Figure 9. 2D multichannel seismic profile (P-1, mentioned in Figure1) over Alcock Rise passes very near to the crescent depression number 1 to 3. Inset map depict mechnism of bottom current for the formation of crescentic depression depression number 2 to 3 east of the intrusive over Alcock Rise (modified after Katari *et al.*, 2015).

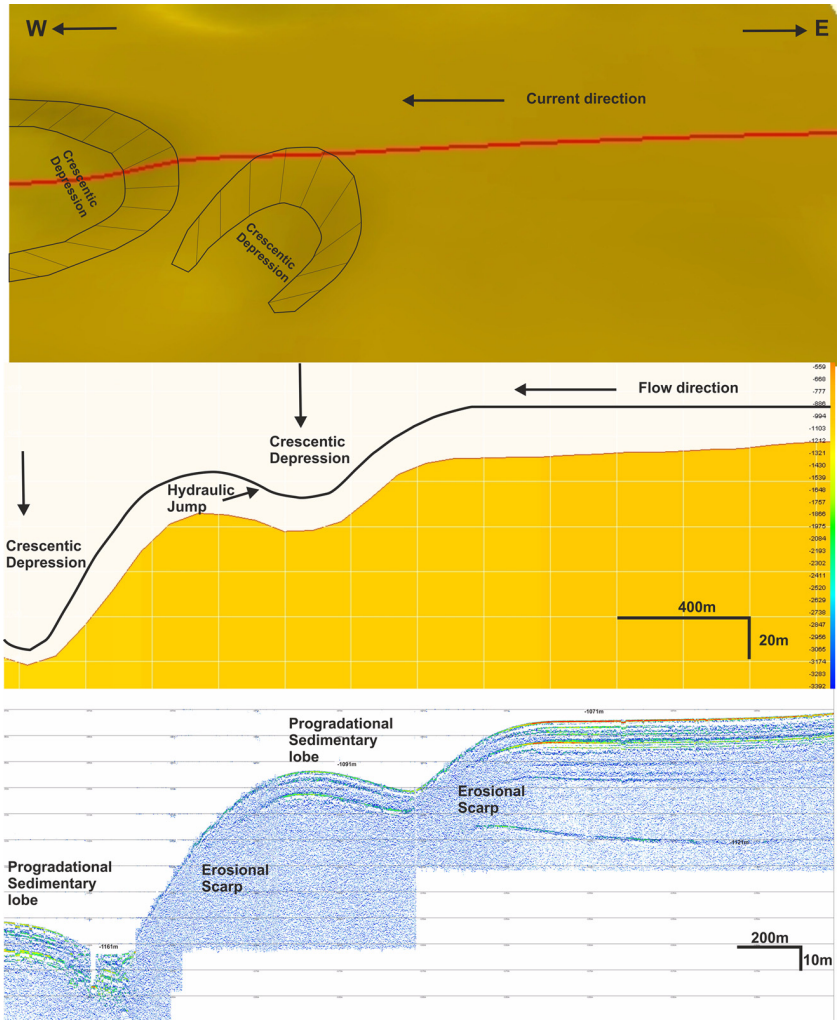


Figure 10. Sketch of SBP profile over crescent depression 25, erosional scarp and depositional lobes indicating current flow direction.

seismic profile P-1(Figure 9). Sediment samples collected from centre of crescent depression 33 consists of coarse sand at the top and very coarse sand with pebbly pockets at the bottom. However, flat top high ridges seen in the seismic profiles are bounded by the normal fault system (Figure 9). However, in western side of the intrusive body seen in Figure 9, there are a series of crescentic depression features as compare to its eastern side (Figure 3).

The interpretation of SPB profiles (around 1000 line km) provided a high-resolution information about the depositional stacking pattern of the sedimentary lobes as well as the information about the fluid migration over crescentic depressions with a penetration up to 40m (Figure 10 and 11). Extensive analysis of the reflector pattern over entire study area reveals that no such fluid movement is breaching out the sediments column. Reflector pattern study also help to identify the erosional scarps and depositional pattern in the internal part of the crescentic depression. Sediments in the area located between the two consecutive crescent depressions number 34 and 36 reveals a stratified reflection pattern (Figure 11). Near crescent depression number 34 and 36, an erosional scarp is seen on both sides of this feature (Figure 11).

**Hydrodynamics of bottom current**

Circulation pattern of surface as well as subsurface current is not well known, only a few indications of eddy (rip) current are given in the National Hydrographic chart. For analyzing current pattern, ADCP was deployed over Alcock Rise where crescent depressions are more concentrated mainly at central part of the study area between -800 and -2000m water depth. This instrument provided the information of current up to 800m water depth and beyond 800m, bottom current information was generated based on the progradational architecture of the sedimentary lobes recorded in the SBP reflectors (Figure 10 and 11).

Overall surface current in the study area was flowing east to southeast direction during the month of February 2017 and June 2017 with magnitude of around 30 cm/s and at places higher magnitude were also recorded over crescentic depression number 5 to 19 and its direction was NE instead of southeast (Supplementary Figure S-1A, S-2 A). Down to -150 m water depth, no such change in the current direction (SE) was observed, only change in magnitude was noticed around 35 cm/s just lower level of the thermocline zone and some places it decreases up to 20 cm/s (Supplementary Figure S-1B, S-2B). Below the -300m water depth (Thermocline zone), overall current direction changes drastically to E-NE instead of SE with recorded magnitude more than 40 cm/s and further it becomes SE over crescentic depression is 36 and 96 at the water depth -800m (Supplementary Figure S-1C, S-2C). However, near depression number 78 to 81, located at -2000 m water depth, current direction at -800m was towards NE to E with decreasing magnitude between 10 to 20 cm/s. Further down up to 800 m water depth, overall current direction was from south to southwesterly with some localized current direction of SE to east with magnitude of around 10 to 25cm/s (Supplementary Figure S-1D, S-2D). Current magnitude analysis from surface water (top) to bottom

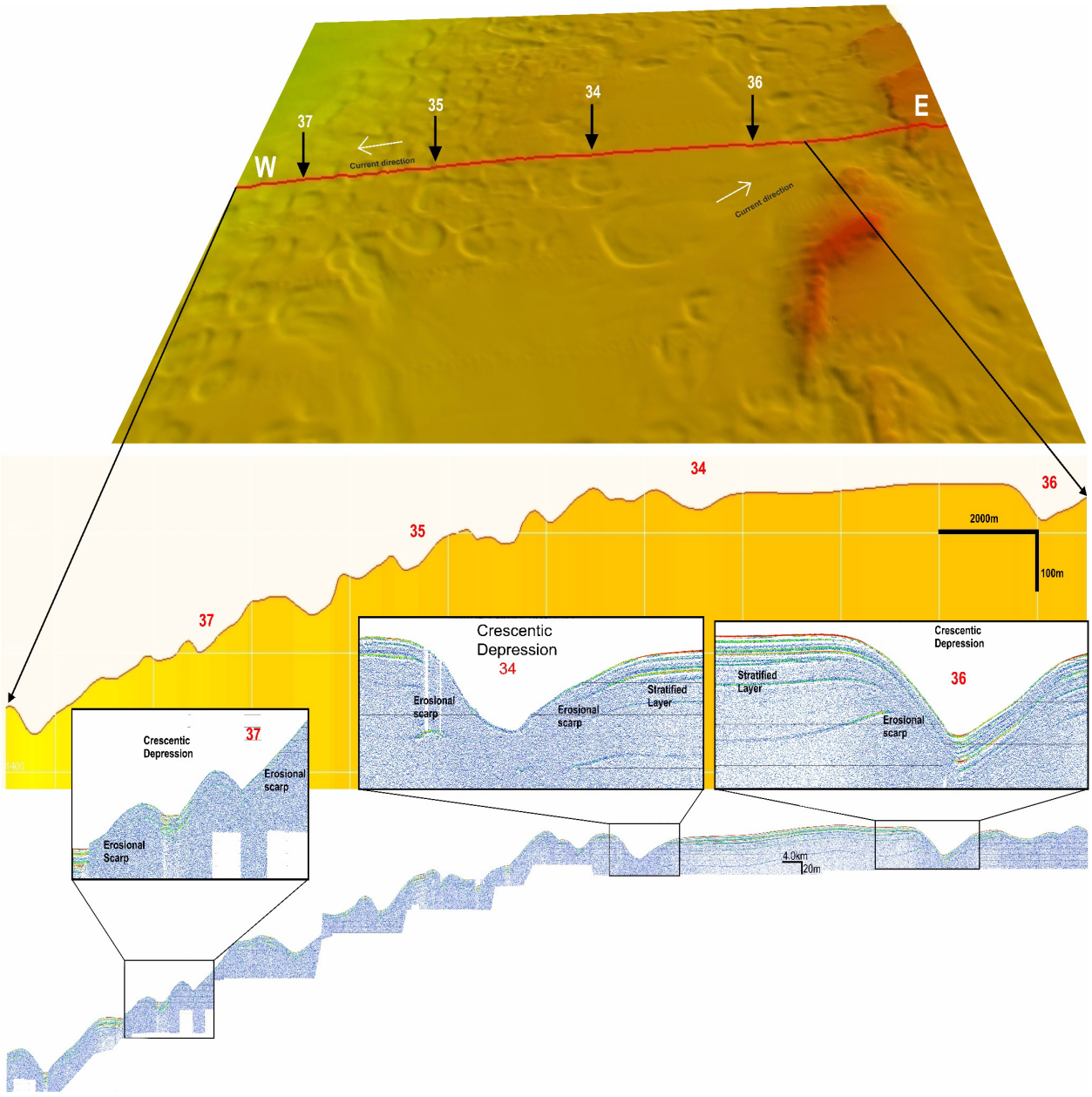


Figure 11. Sketch of SBP profile over western part of the Alcock Rise covering crescent depression 34, 36 and 37, erosional scarp and depositional lobes indicating current flow direction

shows that magnitude increases up to -300m water depth and then decreases up to -800m. Overall, current pattern in the study area does not flow in linear pattern and form a wedge (Supplementary Figure S-1 & S-2). However, bottom current for deeper area (beyond 800m) was hypothetically analyzed to generate the progradational architecture data of the sedimentary lobes with the help of SPB reflectors pattern. This shows erosion in their scarps and deposition in the internal part of the crescentic depression is indicative of flow from the upslope to down slope (Figure 11). In western part of the study area mainly crescentic depression number 22 to 60, the current flow is towards west and northwest. Around crescent depression 72 to 75, overall bottom current pattern is southwesterly. Near the crescent number 34 and 36, reflection pattern shows erosional scarp on both sides indicating flow of the bottom current towards north (Figure 11). Although east of the high land, overall current patterns are towards southeast to east as observed in the reflection pattern. Overall current is radiating in form of arc and oscillating from the steep slope of the guyots and seamounts present over Alcock Rise

## DISCUSSION

Presence of 98 crescentic to elliptical shaped depressions over 50% surface area of Alcock Rise (Figure 3) and its origin was studied with the help of multi-variant relationship between slope and axial ratio, suggests three distinct surface morphological characteristics (Group 1, Group 2 and Group 3, Figure 8). Group 1 and Group 3 fall in the two extreme direction of elongation with respect to Group 2. Majority of the Group 2 located at the NW part of Alcock Rise compare to Group 1 and Group 3, this implies that normal fault controls the overall shape and steepness of their escarpments over Alcock Rise (Figure 3), similar set of normal fault were also observed in the magnetic anomaly map of Dutta *et al.* (2017). Similarly, EH and EW data also supports above observations, which suggest a non-linear relationship of the shape and size irrespective of their location. Moreover, it also found that opening of the crescent arc is independent of the general gradient of the area clearly indicate the role of underlying tectonics features in association with bottom current pattern over Alcock Rise.

### Tectonic control

Morphotectonic structure over Alcock Rise is developed as a result of transtensional fault system between the two dextral transform faults namely SF in association with CAT in the east and WAF in the west (Figure 1). Number of step normal faults also developed within the Alcock Rise following the extensional horse-trail of the SF (Diehl *et al.*, 2013) which later filled up by sediment and subsequently faulted/displaced in form of flower structure as observed in the seismic profile, these flower structures within the soft sediment depict present day neotectonic active. Evidence of neotectonic activity was further supported by the presence of 2004 earthquake epicentre over Alcock Rise (Diehl *et al.*, 2013; Figure 1). Along these step faults, several series of NE-SW trending guyots and seamounts system formed by the volcanic intrusion were also observed which might have provided conduit for magma movement (Figure 9). Similar observation is also corroborated with study of Goli and Pandey (2014), where they mentioned similar set of fault trend and volcanic intrusion over northern part of Alcock rise. So, both observations depict that a series of NE-SW trending normal fault system is controlling overall geomorphology of the Alcock Rise and NE-SW fault system represent the path of remnant strike of SF system (Figure 1, Diehl *et al.*, 2013). Kinematics of the strike slip faults developed transtensional regime and produced classic 'rhomboid' structure and normal faults to the Alcock Rise suggest overall asymmetric nature in terms of basin (Figure S3). Geometry of seamount and guyot system changes from south to north, in south trend of the seamount is NE-SW, become NNE-SSW, and ultimately become parallel to the strike of transform fault (WAF) in NW part of the Alcock Rise (in Curray 2005, marked as down thrown block; Figure 3 and Figure S3). This change in orientation of the seamounts and guyots system may also correspond to the overall dextral movement of the SF and clockwise rotation of Alcock block (Curray, 2005). Overall dextral movement and rotation is creating local transpression along with transtension and one of the possible reasons for development of minor folds at the margin of the fault plane and also reactivating preexisting active faults within the sediment layers (Figure 9 and S3, Eguchi *et al.*, 1979; Curray, 2005; Cochran, 2010; Diehl *et al.*, 2013). Diehl *et al.* (2013) reported several seismic events during 1983, 2003 and 2004 earthquakes along the newly developed normal fault created by extension at 14˚N and over Alcock Rise (Figure 1). Therefore, these seismic events over Alcock Rise may have also triggered slump along the newly formed weaker zone as well as earlier formed crescentic structures over sea floor. This observation was also corroborated from the study of the spade core sediment which contained pockets of pebbles along with coarse sand reveals deposition of poorly sorted sediment by slump related event. Therefore, the combination of faulting and slumping could be one of the possible reasons for the formation of crescentic to semicircular geomorphic structures over Alcock Rise (Figure 10 and Figure 11). Apart from erosion and slump, there is no signature of fluid migration activity is noticed in the sub bottom reflector data. Even though, we cannot rule out the possibility of fluid migration related activity, but in present study could not find any such evidence from the SBP as well as seismic data. So, present study indicates that these crescentic structures over Alcock Rise are formed in association with tectonics and bottom current activity.

### Hydrodynamic model of Bottom Current

Hydrodynamic model for deep-water circulation pattern in Andaman Sea particularly over Alcock Rise is still ambiguous. Use of ADCP for current pattern analysis over the Alcock Rise suggest very erratic current and exhibit multidirectional flow above and below the thermocline zone, with both change in direction and magnitude irrespective of overall general slope (Supplementary Figure S1, S2). Similar observation was recorded in the study of internal wave study by Osborne and Burch (1980), Chatterjee *et al.* (2017), and Sun *et al.* (2019). According to them, unexpectedly large amount of internal wave activity noticed year-round in the northern Andaman Sea. The waves manifest themselves as four groups of internal

wave packets propagating southeast and southwest direction and the bottom topography features mainly control its variability. Martin (2011) also noticed similar observation in the study of surf current pattern analysis over Phuket, Thailand. According to him, it is largely controlled by the presence of number structural features that dissipate wave energy. This trend is also observed during current analysis, all current direction was SE in surface and SW direction below -300m with some localized north and northwest current at places around ridges suggests continuous change in the current direction and magnitude towards bottom imply eddy current pattern. Similar, eddy current behavior was also noticed by the Chatterjee *et al.*, (2017) in north and south of MC. Such erratic internal bottom current over topographic highs (Alcock Rise) might erode sediment from weaker zone, mainly from the margin of crescent and deposits in centre of the depression. This observation is supported by the recovery of very coarse grained sediment with pocket of rock fragments from center of the depression indicates sediment was deposited when bottom energy regime was very strong.

However, detailed bottom current interpretation beyond 800m is lacking around Alcock Rise due to data constraint in ADCP. So it is hypothetically made based on the progradational architecture of sedimentary lobes data generated from the sub bottom profiler reflector. Progradational architecture of sedimentary lobes is indicative of deposition towards internal part of the crescentic depressions and coeval with upslope erosion of their scarps (Duarte *et al.*, 2010). This happens when gradient changes and water loses its linear flow and forms supercritical flow pattern (hydraulic jump; Figure 9). This is only possible due to presence deep sea bottom current, which would be responsible for simultaneous localized erosion and deposition (Fildani *et al.*, 2006; Normark *et al.*, 2009; Duarte *et al.*, 2010). Similar observation also noticed through SPB reflector pattern study that reveals upslope erosion in their scarps with deposition in the internal part of the crescentic depression (Figure 11). Based on the reflector interpretation study, it observed that overall flow over Alcock Rise was mainly in the west and southwest direction at western part of the study area and northerly at the central near to depression 33 to 47. So, overall bottom current data generated over Alcock Rise through SBP reflectors are matching very well with internal soliton current analysis data presented by the Osborne and Burch (1980); Chatterjee *et al.* (2017) and Sun *et al.* (2019). They have documented two directional flows in Andaman Sea at various levels and also pointed out another additional source of strong internal soliton pockets current generation from topographic highs by the tidal oscillation.

**Relationship between active tectonics and bottom current**

Based on above discussion, a model was prepared which explains the role of tectonics and bottom current in formation of crescentic features (Figure S4). Sediment deposited over Alcock Rise was first intersected by the fault generated due to the effect of transtensional regime prevailed in the area and created weak plane within the sediment column. These weak planes were acting as a pathway for bottom current to facilitate the formation the crescent shape structure within the sediment. Later, first formed elliptical crescent shape features along fault margin transformed into semicircular shaped geometry by continuous modification through the bottom current activity over Alcock Rise (Figure S4). This observation is supported by seismic interpretation as mentioned in the Diehl *et al.* (2013), where it is largely controlled by active normal fault (Figure 9). Any frequent movement along these faults induced slumping and scouring of the unconsolidated material, these scour material are eroded by the bottom current, similar observation were also recorded in the study of Duarte *et al.* (2010) and Garcia *et al.* (2015) in Gulf of Cadiz. Seismic data and morphometric analysis also suggest that most of the well-developed or nearly semi-circular crescent structures were formed earlier compare to the recently formed crescentic structure at western margin. This type of well-developed depression mainly located in the central portion of the area, here early formed crescentic structure is under continuous compression and their CW slightly increases. Afterward, bottom current gradually erodes the sediment from the margin of the depression by giving utmost semicircular shape as depicted in Figure S4. It is also observed that crescentic depressions mainly 72 and 73 (Figure 3) are more elongated. This might be because these structures were formed earlier and subsequently modified by the NE-SW trending fault system in association with lateral movement of bottom current, similar internal bottom current activity at various depths in Andaman Sea is also reported in the study of Chatterjee *et al.* (2017) and Sun *et al.* (2019) as well. It is also observed that the concentrations of crescentic structures are more along the western slope where the step faults are present (Figure 13 and Figure11) and it also correspond to the flow of the internal bottom current direction (Chatterjee *et al.* (2017) and Sun *et al.* (2019). Structures along NW margin have longer CL compare to CW, this might be possible due to their closer affinity with respect to normal faults over NW side of the Alcock Rise. Therefore, tectonically controlled gradient along with bottom current provide a simpler explanation for the formation of crescent shape structure over Alcock Rise of Andaman Sea.

## CONCLUSION

Presence of crescentic to elliptical shaped depressions recognized in the swath bathymetry data over Alcock Rise for first time. Study of geomorphological parameters of these features revealed three distinct groups (Group 1, Group 2 and Group 3) and majority of the structure have larger CL and falling over the step faults. Therefore, in Alcock Rise, tectonics play a major role for their formation and subsequently supercritical bottom current flow later modified the entire shape of the crescent. So tectonics and bottom current provides a clue for the formation of these crescent structures over Alcock Rise, Andaman Sea.


## ACKNOWLEDGEMENT

The authors are grateful to A. V. Gangadharan, Deputy Director General, M&CSD, ER, GSI and A. K. Huin, Director ER, GSI for their valuable suggestion to improve the quality of the work. Authors acknowledge their sincere thank to Kaberi Banerjee, Director for supervising the project of SR-023. Authors also take this opportunity to express heartfelt gratitude to Chief scientists Anjaneyulu Katari, Director; Subhankar Dutta, Director and Dr. C.V. Gopalan, Suptdg., Geologist for planning and execution of the project SR-001(2014-15/MGR/ER/SR/2014/001), SR-023 (M1AMCS-SMM/NC/ER/2016/5627) and SR-038 (M1AMCS-SMM/NC/ER/MCSD-EC-1/2017/13953). Authors also thankful to the participants of the above cruises for their dedication and hard work during acquisition of the MBES data. Special thanks to the participant of the cruise SR-001 for Seismic data processing. Also thanks to Dr. Lukram I. Meetei; Senior Geophysicist and Kaushal Kumar, Geophysicist for their technical input during the preparation of the figure. Special thanks to Prof. Michele Rebesco, Istituto Nazionale di Oceanografia e di Geofisica Sperimentale for valuable suggestion for improving the manuscript.


## REFERENCES


Bonnel, C., Dennielou, B., Droz, L., Mulder, T., Berne, S., 2005. Architecture and depositional pattern of the Rhône Neofan and recent gravity activity in the Gulf of Lions (western Mediterranean). *Marine and Petroleum Geology,* 22: 827–843.

Bulat, J., Long, D., 2001. Images of the seabed in the Faroe–Shetland Channel from commercial 3D seismic data. *Marine Geophysical Research,* 22: 345–367.

Casalbore, D., Romagnoli, C., Bosman, A., Chiocci, F.L., 2014. Large-scale seafloor waveforms on the flanks of insular volcanoes (Aeolian Archipelago, Italy), with inferences about their origin. *Marine Geology,* 355: 318–329.

Casalbore, D., Romagnoli, C., Pimentel, A., Quartau, R., Casas, D., Ercilla, G., Hipólito, A., Sposato, A., Chiocci, FL., 2015. Volcanic, tectonic and mass-wasting processes offshore Terceira Island (Azores) revealed by high-resolution seafloor mapping. *Bulletin of Volcanology:* 77, 24.

Chatterjee, A.D. Shankar, J.P. McCreary, P.N. Vinayachandran, and Mukherjee A., 2017. Dynamics of Andaman Sea circulation and its role in connecting the equatorial Indian Ocean to the Bay of Bengal, *J. Geophys. Res. Oceans,* 122, doi:10.1002/2016JC012300.

Cheng, X., S.P. Xie, J. P. McCreary, Y. Qi, and Y. Du (2013), Intraseasonal variability of sea surface height in the Bay of Bengal, *J. Geophys. Res. Oceans,* 118, 816–830, doi:10.1002/jgrc.20075.

Cochran, J.R., 2010. Morphology and tectonics of the Andaman Forearc, northeastern Indian Ocean, *Geophysical Journal International,* 182(2): 631–651.

Collins, J.A., Molnar, P., Sheehan, A.F., 2011. Multibeam bathymetric surveys of submarine volcanoes and mega-pockmarks on the Chatham Rise, New Zealand, *New Zealand Journal of Geology and Geophysics*, 54(3): 329-339.

Curray, J.R., Moore, D.G., Lawver, L.A., Emmel, F.J., Raitt, R.W., Henry, M., and Kieckhefer, R., 1979. Tectonics of the Andaman Sea and Burma. *American Association of Petroleum Geologists mem,* 29: 189–198.

Curray, J.R., 2005. Tectonics and history of Andaman sea region. *Journal of Asian Earth Sciences*, 25, 187-232.

De, L.J., Eggenhuisen, J.T., Cartigny Matthieu, J.B., 2016. Morphodynamics of submarine channel inception revealed by new experimental approach. *Nature communications*. 7, 10886.

Diehl, T.F.W., Cochran, J.R., Kamesh Raju, K.A., Seeber, L., Schaff, D., Engdahl, E.R., 2013. Back-arc extension in the Andaman Sea: Tectonic and magmatic processes imaged by high-precision teleseismic double-difference earthquake relocation*, Journal of Geophysical Research: Solid Earth:* 118.

Duarte, P., Terrinha, F.M., Rosas, V., Valadares, L.M., Pinheiro, L., Matias, V., Magalhaes, C.R., 2010. Crescent-shaped morphotectonic features in the Gulf of Cadiz (offshore SW Iberia). *Marine Geology.* 271: 236-249.

Dutta, S., Madhupriya N., Gunasekharan S., Resmi S., Tripathi S. K., Anwar D., Meitei S I., Jishnu B. K., Nagasundaram M., Singh K. A., Amarnath, Marda R., Rambabu P., 2017.Report on study of morphological and tectonicsetup of northeast Andaman Sea, Geological Survey of India, unpublished report.

Eguchi, T., Uyeda, S., Maki, T., 1979. Seismotectonics and tectonic history of the Andaman Sea. *Tectonophysics*. 57(1): 35–51.

Faugeres, J.C., Mezerais, M.L., Stow, D.A.V., 1993. Contourite drift types and their distribution in the North and South Atlantic Ocean basins. *Sedimentary Geology,* 82: 189-203.

Fildani, A., Normark, W.R., Kostic, S., Parker, G., 2006. Channel formation by flow stripping: large-scale scour features along the Monterey East Channel and their relation to sediment waves. *Sedimentology* 53: 1265-1287.

Garcia, M., Hernández-Molina, F.J., Alonso, B., Vazquez, J.T., Llave, E., Casas, D., 2015. Erosive sub-circular depressions on the Guadalquivir Bank (Gulf of Cadiz): Interaction between bottom current, mass-wasting and tectonic. *Marine Geology,* http://dx.doi.org/10.1016/j.margeo.2015.10.004

Garcia, M., Hernandez-Molina, F.J., Llave, E., Stow, D.A.V., Leon, R., Fernandez-Puga, M.C., Diaz del Rio, V., Somoza, L., 2009. Contourite erosive features caused by the Mediterranean Outflow Water in the Gulf of Cadiz: Quaternary tectonic and oceanographic implications. Marine Geology, 257: 24-40.

Goli, A., Pandey, D.K., 2014. Structural Characteristics of the Andaman Forearc Inferred from Interpretation of Multichannel Seismic Reflection Data. *Acta Geologica Sinica.* 88(4): 1145-1156.

Hanquiez, V., Mulder, T., Lecroat, P., Gonthier, E., Marches, E., Voisset, M., 2007. High resolution seafloor images in the Gulf of Cadiz, Iberian Margin. *Marine Geology.* 246:42-59.

Hernández-Molina, F.J., Llave, E., Preu, B., Ercilla, G., Fontan, A., Bruno, M., Serra, N., Gomiz, J.J., Brackenridge, R.E., Sierro, F.J., Stow, D.A.V., García, M., Juan, C., Sandoval, N., Arnaiz, A., 2014a. Contourite processes associated with the Mediterranean outflow water after its exit from the Strait of Gibraltar: global and conceptual implications. *Geology*, 42: 227-230.

Hernández-Molina, F.J., Llave, E., Stow, D.A.V., García, M., Somoza, L., Vázquez, J.T., Lobo, F.J., Maestro, A., Díaz del Río, V., León, R., Medialdea, T., Gardner, J., 2006. The contourite depositional system of the Gulf of Cádiz: a sedimentary model related to the bottom current activity of the Mediterranean outflow water and its interaction with the continental margin. *Deep-Sea Research*, 53: 1420-1463.

Hernández-Molina, F.J., Serra, N., Stow, D.A.V., 2010. Along-slope oceanographic processes and sedimentary products around Iberia. *Geo-Temas* 11: 69-70.

Hillman, J.I., Ingo K., Ingo, A.P., Andrew, R.G., Jens S.D., Joerg, B., 2018. The influence of submarine currents associated with the Subtropical Front upon seafloor depression morphologies on the eastern passive margin of South Island, New Zealand. *New Zealand Journal of Geology and Geophysics.* 61(1): 112-125.

Hovland, M., 1989. The formation of pockmarks and their potential influence on offshore construction *Quarterly Journal of Engineering Geology and Hydrogeology.* 22: 131-138.

Hsu M K, Hsieh C H, Ho C R, *et al*. 2014. Nonlinear internal waves in the Andaman Sea. *Journal of Photogrammetry and Remote Sensing,* 18(3): 161–173.

Hyder, P., Jeans, D.R.G., Cauquil. E., Nerzic, R., 2005. Observations and predictability of internal solitons in the northern Andaman Sea. *Applied Ocean Research*, 27(1): 1–11, doi:10.1016/j.apor.2005. 07.001.

Jacob, A., Covault, S.K., Charles, K.P., Holly, F.R., Fildan, A., 2014. Submarine channel initiation, filling and maintenance from sea-floor geomorphology and morphodynamic modelling of cyclic steps. *Sedimentology* 61: 1031–1054.

Judd, A.G., Hovland, M., 2007. *Seabed fluid flow: The impact of geology, biology and the marine environment:* Cambridge University Press.

Kamesh Raju, K.A., Ramprasad, T., Rao, P.S., Ramalingeswara Rao, B., Varghese, J., 2004. New insights into the tectonic evolution of the Andaman basin, northeast Indian Ocean. *Earth Planet. Sci. Lett.* 221, 145–162. https://doi.org/10.1016/S0012-821X(04)00075-5.

Kamesh Raju, K.A. 2005. Three-phase tectonic evolution of the Andaman backarc basin. *Current Science,* 89(11): 1933-1937.

Katari, S.A., Chakravarthy, D., Biswas, S.C., Das, P.C., Nandi, B.K., Banerjee, D., Mukopadhyay, R., Meetei, L.I., Nisha, N.V., Pillai, R., Mashod, P.A., Verma, S.K., Routroy, S., Jha, A.K., Ganesh, K., 2015. Study of tectonic setup of northern Andaman Sea by Multi-Channel 2D seismic survey. Geological survey of India FSP Report.Unpublished.

King, L.H., Maclean, B., 1970. Pockmarks on the Scotian Shelf. *Geological Society of America Bulletin.* 81: 3141-3148.

Laberg, J.S., Dahlgren, T., Vorren, T.O., Haflidason, H., Bryn, P., 2001. Seismic analyses of Cenozoic contourite drift development in the northern Norwegian Sea. *Mar. Geophys. Res.* 22, 401-416.

Llave, E., Hernández-Molina, F.J., Ercilla, G., Roque, C., Van Rooij, D., García, M., Juan, C., Mena, A., Brackenridge, R., Jané, G., Stow, D.A.S., Gómez-Ballesteros, M., 2015. Bottom current processes along the Iberian continental margin. *Boletín Geológico y Minero,* 126 (2-3): 219-256.

Maldonado, A., Barnolas, A., Bohoyo, F., Galindo-Zaldivar, J., Hernández-Molina, J., Lobo, F., Rodríguez-Fernández, J., Somoza, L., Vázquez, J.T., 2003. Contourite deposits in the central Scotia Sea: the importance of the Antarctic Circumpolar Current and the Weddell Gyre flows. *Palaeogeography, Palaeoclimatology, Palaeoecology.* 198A: 187-221.

Martin, S.A., 2011. Surf Science of the Andaman Sea - Part I A Surfer's Guide to Wind, Water & Waves:42-45 *thaisurfrider.com.*

McCaffrey, R., 1992: Oblique plate convergence, slip vectors, and fore-arc deformation, *Journal of Geophysical Research* 97: 8905–8915, doi:10.1029/92JB00483.

Mohanty, S., Devendra, R.A., 2017. Numerical simulation of internal waves in the Andaman Sea. In: EGU General Assembly 2017. Vienna, Austria: EGU.

Morley, C.K. 2017.Cenozoic rifting, passive margin development and strike-slip faulting in the Andamans sea: a discusiion of established v. new tectonic model, *Geological Society, London, Memoirs.,* 47:27-50.

Morley, C.K., Alvey, A., 2015. Is spreading prolonged, episodic or incipient in the Andaman Sea? Evidence from deepwater sedimentation. *Journal of Asian Earth Science*. 98: 446-456.

Mulder, T., Voisset, M., Lecroart, P., Le Drezen, E., Gonthier, E., et l'equipe embarqué e Cadisar, 2006. The western part Gulf of Cádiz: interaction between contour and turbidity currents. *Geo-Marine Letter.* 26:31–41.

Normark, W.R., Paull, C.K., Caress, D.W., Ussler III, W., Sliter, R., 2009. Fine-scale relief related to Late Holocene channel shifting within the floor of the upper Redondo Fan, offshore Southern California. *Sedimentology.* 56:1690–1704.

Osborne A. R. and Burch T. L. 1980: Internal Solitons in the Andaman Sea, *Science,* vol. 208, 451-460.

Pickering, K.T., Hiscott, R.N., Hein, F.J., 1989. Deep marine environments. *Clastic Sedimentation and Tectonics*. Unwin Hyman Ltd, London.

Potemra, J.T., Luther, M.E., and O'Brien, J.J., 1991. The seasonal circulation of the upper ocean in the Bay of Bengal, *J. Geophys. Res.,* 96, 12,667–12,683.

Rabinowitz P.D., Ryan W.B.F., 1970. Gravity Anomalies and Crustal Shortening in the Eastern Mediterraneani. *Tectonophysics*, 10:585-608.

Rangin, C., Maw, W., Lwin S.W.N., Mouret, C., Bertrand, G., GIAC scientific party 1999. Cenozoic pull apart basins in central Burma; the trace of the path of India along the western margin of Sundaland, paper presented at European Union of Geosciences conferences, Strasbourg, France.

Rebesco, M., 2005. Contourites. In: Richard, C., Selley, R.C., Cocks, L.R.M., Plimer, I.R. (Eds.), *Encyclopedia of Geology* 4. Elsevier, London, 513–527.

Rebesco, M., Camerlenghi, A., 2008. *Contourites, Developments in Sedimentology.* Elsevier, Amsterdam.

Rebesco, M., Hernández-Molina, F.J., Van Rooij, D., Wåhlin, A., 2014. Contourites and associated sediments controlled by deep-water circulation processes: state of the art and future considerations. *Marine Geology.* 352: 111–154.

Rebesco, M., Stow, D.A.S., 2001. Seismic expression of contourites and related deposits: a preface. *Marine Geophysical Research,* 22: 303–308.

Rensbergen, V.P., Depreiter, D.P.B., Henriet, J.P., 2005. Seafloor expression of sediment extrusion and intrusion at the El Arraiche mud volcano field, Gulf of Cadiz, *Journal of Geophysical Research*. 110:02010.

Rodolfo, K.S., 1969. Bathymetry and marine geology of the Andaman basin and tectonic implications for SE Asia. *Geological Society of America Bulletin*. 80: 1203-1230.

Seeber, L., Cormier, M.H., McHugh, C., Emre, O.P.A., Sorlien, C., 2006. Rapid subsidence and sedimentation from oblique slip near a bend on the North Anatolian transform fault in the Marmara Sea, Turkey. *Geology*, 34(11): 933–936.

Somoza, L., Díaz-del-Río, V., León, R., Ivanov, M., Fernández-Puga, M.C., Gardner, J.M., Hernández-Molina, F.J., Pinheiro, L.M., Rodero, J., Lobato, A., Maestro, A., Vázquez, J.T., Medialdea, T., Fernández-Salas, L.M., 2003. Seabed morphology and hydrocarbon seepage in the Gulf of Cádiz mud volcano area: acoustic imagery, multibeam and ultra-high resolution seismic data. *Marine Geology,* 195: 153-176.

Stow, D. A. V., Faugères, J-C., Howe, J. A., Pudsey, C. J., & Viana, A. R., 2002. Bottom currents, contourites and deep-sea sediment drifts: current state-of-the-art. *Memoirs,* 22: 7-20. https://doi.org/10.1144/GSL.MEM. 2002.022.01.02

Stow, D.A.V., Hernández-Molina, F.J., Llave, E., Sayago-Gil, M., Díaz-del Río, V., Branson, A., 2009. Bed form-velocity matrix: the estimation of bottom current velocity from bed form observations. *Geology* 37: 327-330.

Sun, L., Zhang, J., Meng, J., 2019. A study of the spatial-temporal distribution and propagation characteristics of internal waves in the Andaman Sea using MODIS. *Acta Oceanologica Sinica*, 38(7): 121–128, doi:10.1007/s13131-019-1449-8.

Taira, A., Saito, Y., and Hashimoto, M., 1983. The role of oblique subduction and strike-slip tectonics in the evolution of Japan. In *Geodynamics of the Western Pacific-Indonesian Region*, ed. *TWC Hilde, S Uyeda*, pp. 303–16.Washington, DC: *American Geophysical Union*. 457 pp.

Tripathi, S.K., Banerjee, K., 2016. First record of Limestone rock over Alcock Rise, Andaman Sea, www. gsi.gov.in, November, 1-5.

Van Rooij, D., Iglesias, J., Hernandez-Molina, F.J., Ercilla, G., Gomez-Ballesteros, M., Casas, D., Llave, E., De Hauwere, A., Garcia, G.S., Acosta, J., Henriet, J.P., 2010. The Le Danois Contourite Depositional System: interactions between the Mediterranean outflow water and the upper Cantabrian slope (North Iberian margin). *Marine Geology*. 274: 1-20.

Verdicchio, G., Trincardi, F., 2006. Short-distance variability in slope bed-forms along the Southwestern Adriatic Margin (Central Mediterranean). *Marine Geology,* 234: 271–292.

Viana, A., Rebesco, M., 2007. Economic and paleoceanographic significance of contourites. *Geological Society, London, Special. Publication*. 276.

Viana, A.R., 2008. Economic relevance of contourites. In: Rebesco, M., Camerlenghi, A. (Eds.), Contourites. *Elsevier, Amsterdam*, Developments in *Sedimentology*. 60: 493–510.

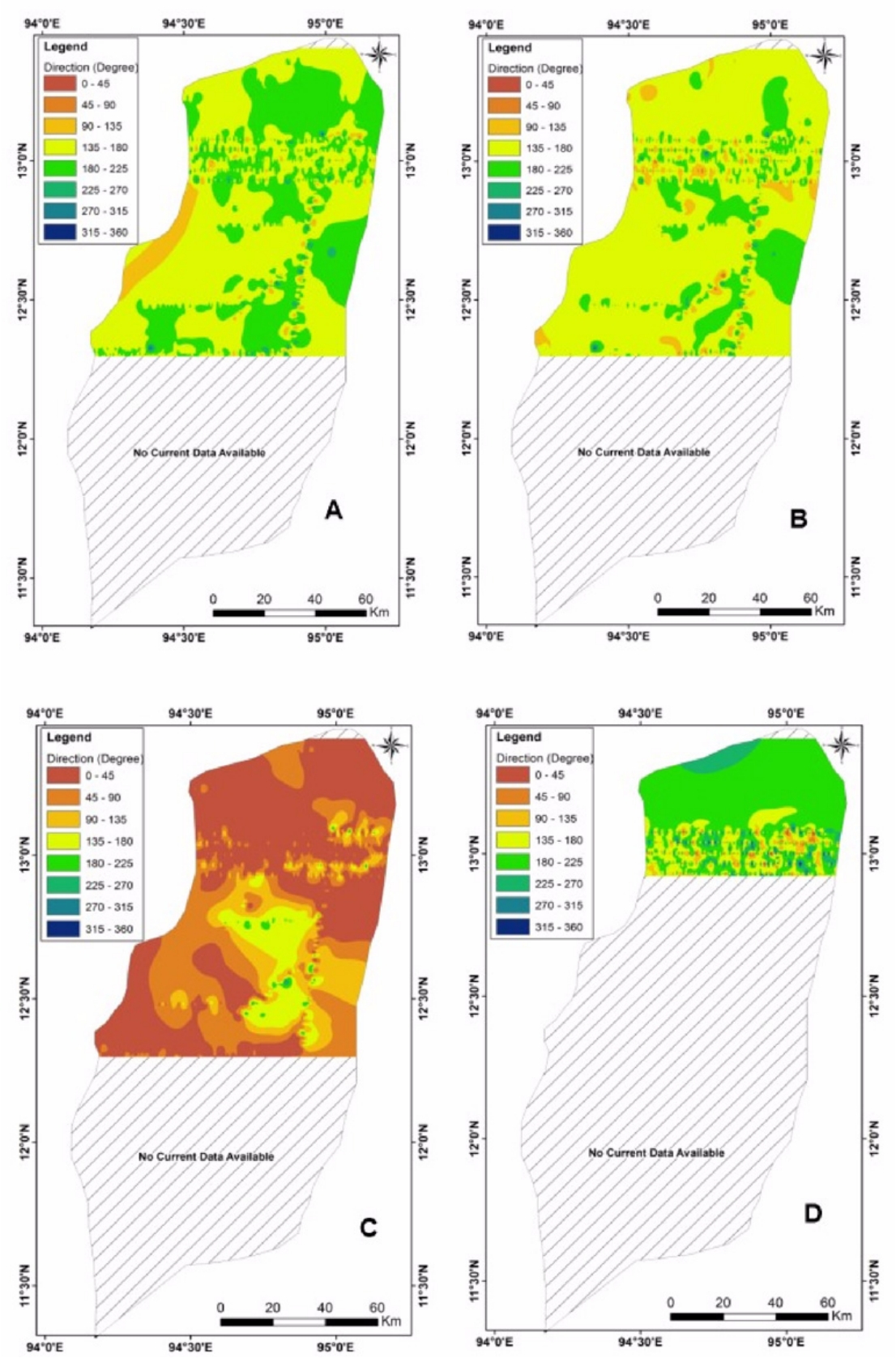


Figure S-1. Current direction over crescent depression, Alcock Rise, Andaman Sea. Where A) surface current B) 150m water depth, C) 300m water depth current direction, D) 800 m water depth current direction.

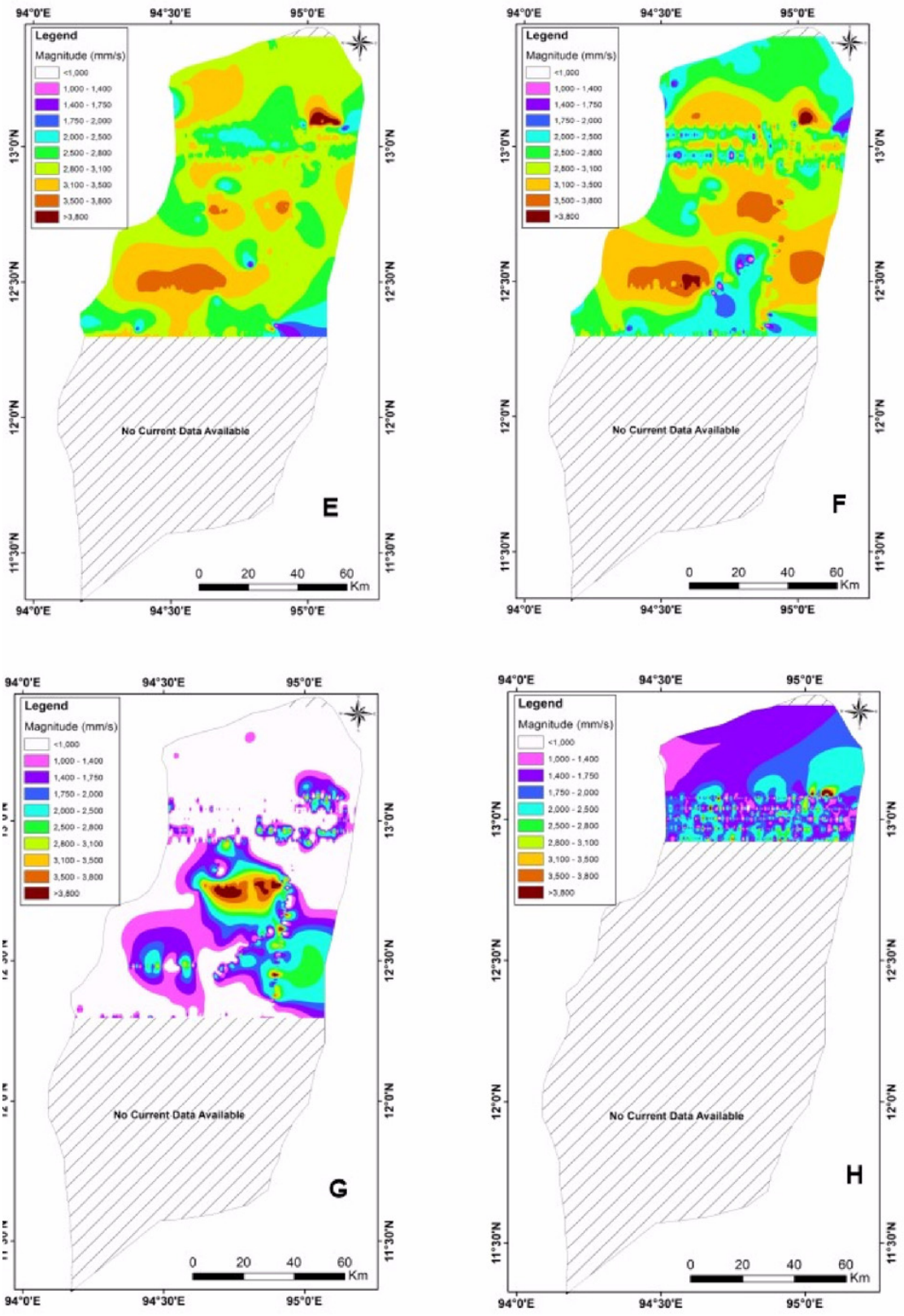


Figure S-2. Magnitude of the current over crescent depression, Alcock Rise, Andaman Sea. Where A) surface magnitude of the current, B) 150m water depth, C) 300m water depth current direction, D) 800 m water depth magnitude of the current.

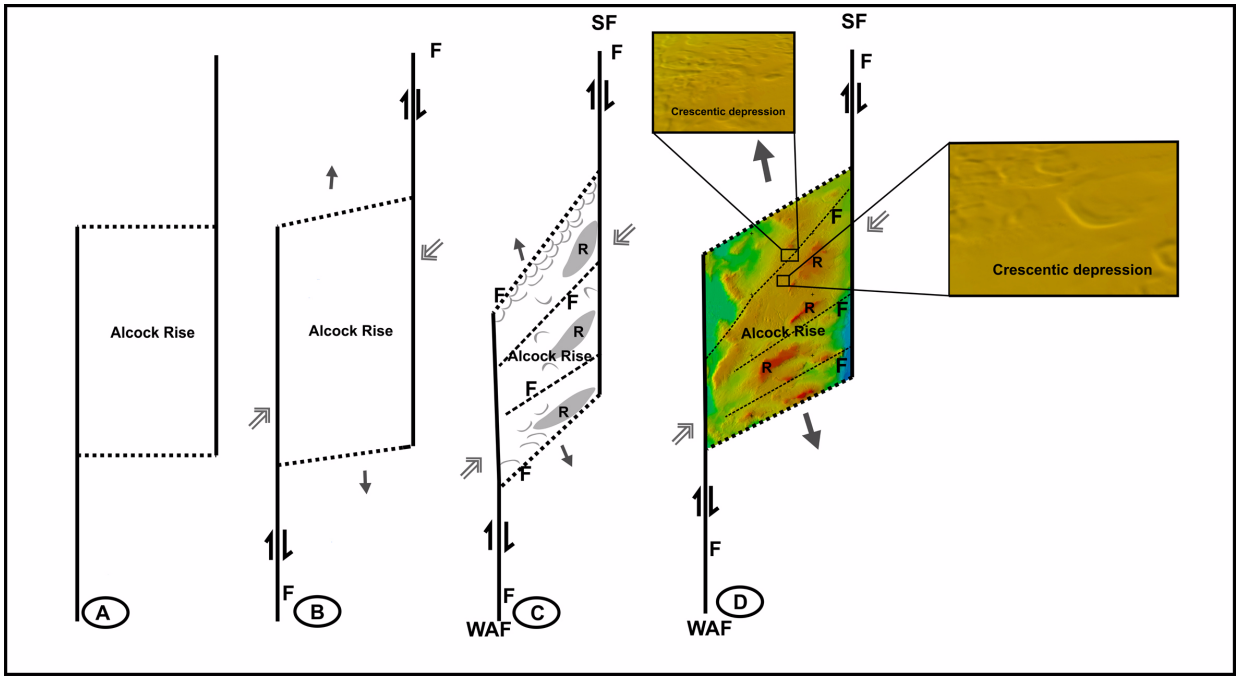


Figure-S3: Block diagram represent the overall transtensional dextral transform fault over Alcock Rise. A) represent the earlier shape of the Alcock Rise before intiation of transtensional regime, B) represent the intiation of strike slip movement and overlap zone of the Alcock, C) represent the present day configuration of based on the interpreation of the multibeam bathymetry shown in D), where a detailed of crescent depression is imaged. Where dash line show the trend of the normal fault, solid black arrow shows the direction of extension and double arrow mark the direction of high angle compression. Abbriviation F= Fault, R= ridge, SF= Saggaing Fault, WAF= West Andaman Fault

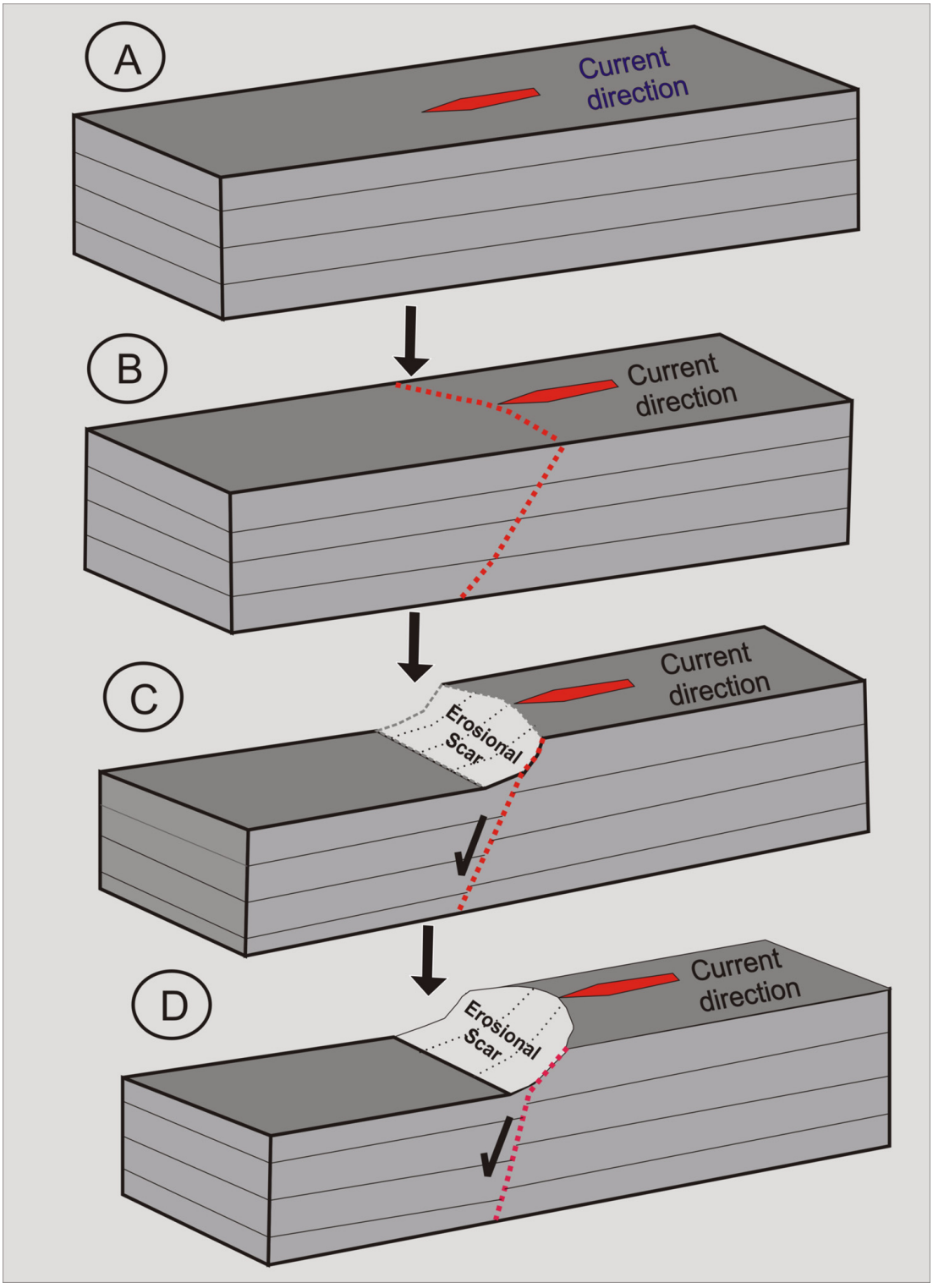


Figure-S4: Representative model explains the role of tectonics and bottom current in formation of crescentic features (Figure S4). A) Sediment pattern over Alcock Rise, B) Deposited sediment was first intersected by the fault generated due to the effect of transtensional regime, C) Along weak plane, bottom current facilitating the formation the crescent shape structure within the sediment. D) Earlier formed elliptical crescent shape features along fault margin transformed into semicircular shaped geometry by continuous modification through the bottom current activity.